

Polarons and phase separation in lanthanum-based manganese perovskites: A ^{139}La and ^{55}Mn NMR study

G. Papavassiliou, M. Fardis, M. Belesi, M. Pissas, I. Panagiotopoulos, G. Kallias, and D. Niarchos
Institute of Materials Science, National Center for Scientific, Research "Demokritos," 153 10 Athens, Greece

C. Dimitropoulos

Institut de Physique Expérimentale, Ecole Polytechnique Fédérale de Lausanne, PH-Ecublens, 1015-Lausanne, Switzerland

J. Dolinsek

"Josef Stefan" Institute, Jamova 39, 61111 Ljubljana, Slovenia

(Received 12 June 1998; revised manuscript received 28 September 1998)

Low-temperature ^{139}La and ^{55}Mn NMR line shape measurements in $\text{La}_{1-x}\text{Ca}_x\text{MnO}_3$ for $0.125 \leq x \leq 0.5$, and $\text{La}_{0.67}(\text{Ca}_{1-y}\text{Ba}_y)_{0.33}\text{MnO}_3$ for $0 \leq y \leq 1$ are shown to directly reflect changes of the structure and of the magnetic state at a local level. For low x values in $\text{La}_{1-x}\text{Ca}_x\text{MnO}_3$ evidence is given about the presence of polaronic lattice distortions. By increasing x , structurally undistorted conductive ferromagnetic (FM) regions are formed indicating a percolative metal to insulator phase transition, whereas for $x=0.5$ the system is shown to break into FM and antiferromagnetic regions in accordance with the predictions of the electronic phase separation model. [S0163-1829(99)04609-3]

I. INTRODUCTION

One of the most challenging problems in the physics of strongly correlated electron systems, concerns the origin of the large negative magnetoresistance in manganese perovskites of the type $\text{La}_{1-x}\text{D}_x\text{MnO}_3$ (L = lanthanide, D = divalent ion). According to theory, doping of antiferromagnetic (AFM) LMnO_3 insulators with mobile e_g holes favors the establishment of ferromagnetic (FM) order, via Hund's coupling between holes and localized t_{2g} spins.¹ Nevertheless, competition between FM and AFM exchange interactions creates a complicated magnetic phase diagram, depending on doping concentration² and the kind of trivalent/divalent cation.³ Detailed studies of the $\text{La}_{1-x}\text{Ca}_x\text{MnO}_3$ family have shown that for $0.15 < x < 0.5$ these systems undergo a phase transition from a high-temperature insulating paramagnetic (PM) to a low-temperature metallic FM phase.² At half filling $x=0.5$, the FM phase becomes unstable against the formation of a low temperature charge ordered AFM phase, and the phase transition route becomes PM-FM-AFM on cooling. Further investigations in $\text{La}_{1-x}\text{Sr}_x\text{MnO}_3$ have shown the presence of a canted AFM phase (AFM with a weak FM component) for $x < 0.1$, and a FM insulating phase for $0.1 < x < 0.15$.⁴ However, the interpretation of the magnetic phase diagram is still controversial. A great debate concerns those regions of the phase diagram, where coexistence of FM and AFM magnetic ordering has been observed. In these regions magnetization,² neutron scattering,⁵ and NMR (Refs. 6 and 7) experiments are explainable either within the framework of a canted AFM state,⁸ or with a mixed two-phase state consisting of FM and AFM regions with high, respectively low, charge carrier concentration.^{9,10} On the other hand, the presence of local Jahn-Teller (JT) distortions, even in the FM phase, implies local variations of the magnetic interactions, which modify the magnetic phase diagram. Recently, the formation of three Mn polaronic clusters in the JT distorted FM phase of $\text{La}_{1-x}\text{Sr}_x\text{MnO}_3$ at low temperatures

was proposed by Louca *et al.*¹¹ in order to explain pulsed neutron diffraction results. Zhou *et al.*¹² suggested that these clusters consist of $\text{Mn}^{3+}\text{-O-Mn}^{4+}\text{-O-Mn}^{3+}$, where the e_g hole is alternately at one of the two Mn^{3+} sites, and is made mobile by a dynamic JT coupling to the oxygen vibrations between Mn atoms. Conductivity in this model is described in terms of connectivity of polaronic networks.

In this paper we examine the microscopic magnetic state of $\text{La}_{1-x}\text{Ca}_x\text{MnO}_3$ for $0.125 \leq x \leq 0.5$ and $\text{La}_{0.67}(\text{Ca}_{1-y}\text{Ba}_y)_{0.33}\text{MnO}_3$ for $0 \leq y \leq 1$ at low temperatures, by using ^{139}La and ^{55}Mn NMR line shape measurements in a zero external magnetic field. The most interesting behavior is shown by $\text{La}_{1-x}\text{Ca}_x\text{MnO}_3$. We present evidence about the presence of a polaronic state related to local JT distortions at low x values, in agreement with the proposition of Louca¹¹ and Zhou.¹² By increasing x conductive FM clusters with suppressed JT distortions are formed, whereas for $x=0.5$ the system appears to break into FM and AFM regions in agreement with the predictions of the phase separation theory.^{9,10}

II. SAMPLE PREPARATION AND CHARACTERIZATION

$\text{La}_{1-x}\text{Ca}_x\text{MnO}_3$ and $\text{La}_{0.67}(\text{Ca}_{1-y}\text{Ba}_y)_{0.33}\text{MnO}_3$ samples were prepared by thoroughly mixing high-purity stoichiometric amounts of La_2O_3 , MnO_2 , CaCO_3 , and/or BaCO_3 . The mixing powders were pelletized and annealed in air at 1300 to 1400 °C, depending on the composition, for 4 days with intermediate grinding and reformation into pellets. Finally, they were slowly cooled to room temperature by turning off the furnace. All samples were then characterized structurally at room temperature with a D500 Siemens x-ray diffractometer, and magnetically with a SQUID magnetometer. The obtained crystallographic and magnetic data were found to be in accordance with literature.

Figure 1 demonstrates magnetization measurements as a function of temperature for $\text{La}_{1-x}\text{Ca}_x\text{MnO}_3$, $x=0.125, 0.33, 0.5$, and $\text{La}_{0.67}\text{Ba}_{0.33}\text{MnO}_3$. The inset presents resistivity vs

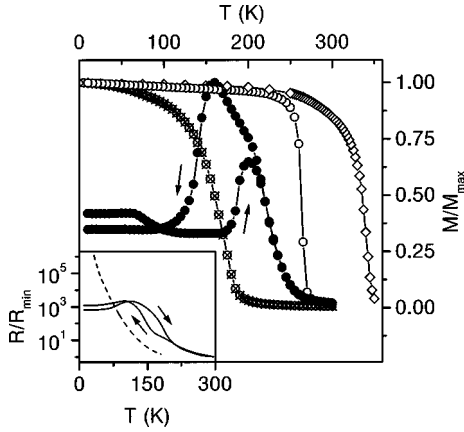


FIG. 1. Magnetization as a function of temperature of $\text{La}_{1-x}\text{Ca}_x\text{MnO}_3$, for $x=0.125$ [$T_c=160$ K (\otimes)], $x=0.33$ [$T_c=265$ K (\circ)], $x=0.5$ [$T_c=225$ K and $T_N=140$ K on cooling, (\bullet)], and for $\text{La}_{0.67}\text{Ba}_{0.33}\text{MnO}_3$ [$T_c=340$ K (\diamond)]. The inset presents resistivity vs T measurements for $x=0.125$ (dashed line) and $x=0.5$ (solid line). In all measurements samples were cooled in zero magnetic field and subsequently measured in a magnetic field of 1000 G. The phase transition temperatures were obtained from the inflection points of the M vs T curves.

T measurements for the insulating $x=0.125$ and 0.5 systems. In all measurements, samples were initially cooled in nearly zero magnetic field and subsequently measured in a magnetic field of 1000 G. The phase transition temperatures (given in the text of Fig. 1) were obtained from the inflection points of the M vs T curves. Special care was taken for the characterization of the $x=0.5$ system because even a slight modification of x or Mn^{4+} content alters magnetization and resistivity dramatically, due to proximity to the FM-AFM phase boundary.¹³ In our $x=0.5$ sample ($T_c \approx 225$ K), the system starts from a nonfully AFM state at low temperatures, attains a magnetization maximum at $T \approx 200$ K ($T_N \approx 180$ K) on heating, and then it drops rapidly to the high-temperature PM phase. On the opposite way (cooling), magnetization accesses a maximum at $T \approx 160$ K, where it starts dropping to the nonfully AFM state ($T_N \approx 140$ K), falling finally to 35% of the maximum value. The difference in the low-temperature magnetization and resistivity values between heating (zero field cooling) and cooling (field cooling), is due to the strong dependence of the magnetic and magnetotransport properties on the magnetic and thermal history of the sample. This effect has been examined systematically in $\text{La}_{0.5}\text{Ca}_{0.5}\text{MnO}_{3+\delta}$ by Xiao *et al.*¹⁴ A further remarkable point is the slight fall of the remnant magnetization at ~ 100 K upon heating, which is absent on the reverse way. A similar effect in a field of 150 G is demonstrated in Ref. 14.

III. NMR RESULTS AND DISCUSSION

Zero external magnetic field NMR probes the local magnetic environment of the resonating nuclei through the hyperfine field $B_{\text{hf}} = (1/\gamma\hbar)A\langle S \rangle$, where A and $\langle S \rangle$ are the hyperfine coupling constant and the average electronic spin, respectively. According to this formula, ^{55}Mn NMR probes the electron spin state of single Mn ions and therefore it is possible to resolve the different Mn charge states, i.e., local-

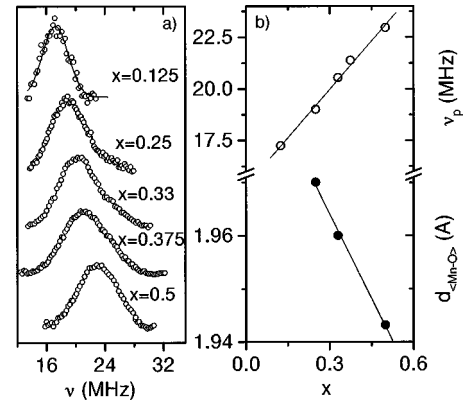


FIG. 2. (a) Zero external magnetic field ^{139}La NMR spectra of $\text{La}_{1-x}\text{Ca}_x\text{MnO}_3$ for $x=0.125, 0.25, 0.33, 0.375,$ and 0.50 at $T=5$ K. (b) The ^{139}La NMR peak frequency ν_p as a function of x at 5 K, and the average Mn-O distance $d_{(\text{Mn-O})}$ as a function of x at room temperature. A similar $d_{(\text{Mn-O})}$ vs x behavior is expected at low temperatures (Ref. 3). Data for $d_{(\text{Mn-O})}$ were taken from Refs. 3, 18, and 19.

ized Mn^{3+} , Mn^{4+} and intermediate FM valence states. On the other hand, ^{139}La NMR ($S=0$), which probes the average spin state of the surrounding Mn octant through transferred hyperfine interactions, is very sensitive to changes of the local Mn spin configuration. Symmetry arguments indicate that $B_{\text{hf}}(\text{La})$ varies from zero value for collinearly AFM ordered Mn octants, to a maximum value for collinearly FM ordered Mn octants.⁸ In the case of a canted AFM state $B_{\text{hf}}(\text{La})$ is partially cancelled and therefore the La NMR frequency is sufficiently lower than in the FM state. Recently, it has been proposed that $B_{\text{hf}}(\text{La})$ arises indirectly via π type overlapping between the Mn t_{2g} , $|3d_{xy}\rangle$, $|3d_{yz}\rangle$, $|3d_{zx}\rangle$, and the oxygen $|2p_{\pi}\rangle$ wave functions, in conjunction with σ bonding of the oxygen with the $|sp^3\rangle$ hybrid states of the La^{3+} ion.⁶ In this picture ^{139}La NMR signal frequency is insensitive to the population of the e_g state and reflects (i) the t_{2g} electron spin ordering of Mn octants, (ii) possible deformations of the Mn-O-Mn bonding, which alter the hyperfine coupling constant A .

The best NMR signal to noise ratio in zero external magnetic field was obtained by using a $2 \mu\text{s}$ -tau- $2 \mu\text{s}$ spin-echo technique and rf power level of the order of $H_1 \approx 0.1$ G, due to the strong rf enhancement created by the oscillating (at rf frequency) electron magnetic moments.¹⁵ For these experimental conditions both ^{139}La and ^{55}Mn NMR signals are shown to originate from domain walls.¹⁶ Previous studies on $\text{La}_{1-x}\text{Ca}_x\text{MnO}_3$, for $x=0.33$ and 0.5 at various rf levels, have shown that ^{139}La NMR signals from domain walls (low rf power) have the same line shape and frequency as signals from domains (high rf power).^{6,16} On the other hand, ^{55}Mn NMR signals of $\text{La}_{0.67}\text{Ca}_{0.33}\text{MnO}_3$ from domains are found to be slightly shifted to lower frequencies in comparison to signals from domain walls, for $T < 80$ K.¹⁶ The origin of this shift has been attributed to difference in hole density between domains and domain walls at low temperatures.¹⁶

Figure 2(a) presents ^{139}La zero external field NMR spectra of $\text{La}_{1-x}\text{Ca}_x\text{MnO}_3$ for $x=0.125, 0.25, 0.33, 0.375,$ and 0.5 at 5 K. For $x=0.125$ the signal is very weak with a

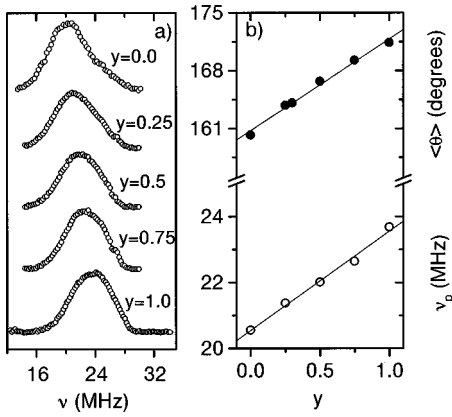


FIG. 3. (a) Zero external magnetic field ^{139}La NMR spectra of $\text{La}_{0.67}(\text{Ca}_{1-y}\text{Ba}_y)_{0.33}\text{MnO}_3$ for $y=0.0, 0.25, 0.50, 0.75,$ and 1.0 at $T=5$ K. (b) The ^{139}La NMR peak frequency ν_p as a function of y at 5 K, and the average $\langle \text{Mn-O-Mn} \rangle$ angle as a function of y at room temperature. A similar $\langle \text{Mn-O-Mn} \rangle$ vs y behavior is expected at low temperatures (Ref. 3). Data for $\langle \text{Mn-O-Mn} \rangle$ were taken from Ref. 20.

symmetric Gaussian line shape located at $\nu \approx 17.5$ MHz. For $x \geq 0.25$ signals are strong and asymmetric, while shifting linearly to higher frequencies. The highest signal frequency is observed for $x=0.5$. This is remarkable as this system is AFM at 5 K, so $B_{\text{hf}}(\text{La})$ should be sufficiently lower than in FM $x=0.25, 0.33,$ and 0.375 systems. The only possible explanation is that even for $x=0.5$ the observed NMR signal is produced in FM ordered regions. In such a case, since $B_{\text{hf}}(\text{La})$ is insensitive to the population of the e_g electron states,¹⁷ the ^{139}La NMR frequency increase may be solely attributed to an increase of the hyperfine coupling constant A . This assertion is supported by neutron scattering experiments in $\text{La}_{1-x}\text{Ca}_x\text{MnO}_3$ (Refs. 3,18,19) which show that the average Mn-O distance $d_{\langle \text{Mn-O} \rangle}$ decreases linearly with x [Fig. 2(b)], whereas the average $\langle \text{Mn-O-Mn} \rangle$ angle remains almost invariant. The decrease of $d_{\langle \text{Mn-O} \rangle}$ increases the Mn-O wave function overlapping and consequently increases the values of A . Recently, Louca *et al.*¹¹ have shown that the decrease of $d_{\langle \text{Mn-O} \rangle}$ as a function of x at low temperatures is due to the increase of the number of short $\langle \text{Mn-O} \rangle$ bonds per Mn ion. This number varies from $N_{\langle \text{Mn-O} \rangle} \approx 4$ for $x=0.0$ (completely JT distorted unit cell) to $N_{\langle \text{Mn-O} \rangle} \approx 6$ for $x \approx 0.35$ (completely undistorted unit cell). However, according to Fig. 2(b) the ^{139}La NMR signal frequency increases linearly up to $x=0.5$, which may indicate the presence of local JT distortions beyond $x=0.35$.

The dependence of the ^{139}La NMR frequency on the Mn-O-Mn bond geometry is further shown in Fig. 3(a), which illustrates ^{139}La NMR line shape measurements in $\text{La}_{0.67}(\text{Ca}_{1-y}\text{Ba}_y)_{0.33}\text{MnO}_3$, for $y=0.0, 0.25, 0.50, 0.75,$ and 1.0 , at 5 K. All these systems are FM at 5 K and they have a constant $\text{Mn}^{4+}/\text{Mn}^{3+}$ ratio. This minimizes the number of parameters, which may influence the ^{139}La NMR signal. XRD experiments at room temperature have shown that the $\langle \text{Mn-O-Mn} \rangle$ angle increases with y from 160° to 171° , whereas within experimental error, $d_{\langle \text{Mn-O} \rangle}$ remains constant with value 1.96 \AA .²⁰ As a result, by Ba substitution the structure comes closer to the ideal perovskite with less tilted

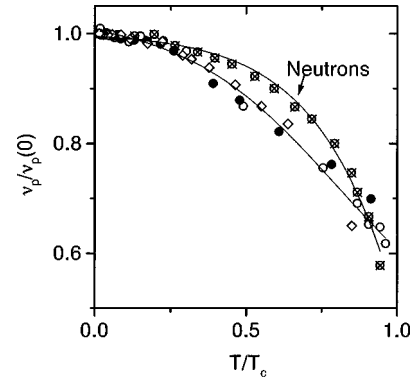


FIG. 4. The normalized ^{139}La NMR peak frequency vs T/T_c of $\text{La}_{1-x}\text{Ca}_x\text{MnO}_3$, $x=0.33$ (\circ), 0.5 (\bullet), and $\text{La}_{0.33}\text{Ba}_{0.67}\text{MnO}_3$ (\diamond). For reasons of comparison the normalized neutron scattering (110) FM peak intensity vs T/T_c of $\text{La}_{0.67}\text{Ca}_{0.33}\text{MnO}_3$ (\otimes) from Ref. 18 is also presented. Solid lines are guides to the eye.

MnO_6 octahedra. This is reflected in the ^{139}La NMR spectra of Fig. 3, where it is shown that by increasing y spectra become more symmetric while shifting linearly to higher frequency.

The above results imply that in both $\text{La}_{1-x}\text{Ca}_x\text{MnO}_3$ and $\text{La}_{0.67}(\text{Ca}_{1-y}\text{Ba}_y)_{0.33}\text{MnO}_3$, (i) the observed ^{139}La NMR signals are produced in FM ordered regions, (ii) the systematic frequency increase with x , (y) is due to decrease of $d_{\langle \text{Mn-O} \rangle}$ (increase of $\langle \text{Mn-O-Mn} \rangle$). This has the following consequence: In the tight-binding approximation the conduction bandwidth W , and therefore the e_g hole hopping integral $t \propto W$, depends strongly on both $d_{\langle \text{Mn-O} \rangle}$ and $\langle \text{Mn-O-Mn} \rangle$ through the Mn $3d$ and the oxygen $2p_\pi$ overlapping integrals. This is formulated empirically as $W \propto \cos \omega/d_{\langle \text{Mn-O} \rangle}^{3.5}$,³ where $\omega = \frac{1}{2}(\pi - \langle \text{Mn-O-Mn} \rangle)$. According to this formula the ^{139}La NMR frequency is proportional to hole mobility at a local level.

It is thus reasonable to assume that the appearance of a high frequency tail in the ^{139}La spectra of $\text{La}_{1-x}\text{Ca}_x\text{MnO}_3$ for $x \geq 0.25$, as shown in Fig. 2(a), indicates the formation of FM clusters with reduced JT distortions and enhanced hole mobility. For the FM and insulating $x=0.125$ no high frequency tail is observed. By increasing x the high frequency tail grows, which indicates that FM clusters with enhanced hole mobility grow in size and number with x . In this picture conductivity is established by a percolation transition. For $x=0.5$ the spectrum is symmetric and shifted at the position of the high frequency tail, which shows the presence of conductive FM islands imbedded into the insulating AFM matrix. According to Kashin and Nagaev,²¹ for carrier concentration $x > x_c = 4J_{\text{AFM}}/J_{\text{FM}}$ degenerate magnetic semiconductors may split into regions with increased (FM) and decreased (AFM) hole density. Apparently, this condition is fulfilled for $x=0.5$.

Further evidence about the formation of pure FM regions in the AFM phase of the $x=0.5$ system is presented in Fig. 4, where the normalized ^{139}La NMR peak frequency of $\text{La}_{1-x}\text{Ca}_x\text{MnO}_3$ for $x=0.33, 0.5$ and $\text{La}_{0.67}\text{Ba}_{0.33}\text{MnO}_3$ is plotted as a function of T/T_c . For reasons of comparison the (110) FM peak intensity vs T/T_c in $\text{La}_{0.67}\text{Ca}_{0.33}\text{MnO}_3$ from

Ref. 18, measured by neutron scattering, is also presented. It is observed that in all three samples the ^{139}La NMR frequency curves coincide, whereas they deviate considerably from the neutron scattering curve. This deviation is due to the fact that neutron scattering measures directly $\langle S \rangle$, whereas ^{139}La NMR depends heavily on structural parameters, which vary considerably by increasing temperature.¹¹ Another notable property of $\text{La}_{0.5}\text{Ca}_{0.5}\text{MnO}_3$ is that the signal frequency varies continuously with temperature across the AFM-to-FM phase transition temperature, despite the large abrupt change of the a, b, c , lattice constants at T_N .¹⁹ This is probably related with the fact that lattice constants change in such a way that the unit cell volume varies smoothly with temperature across T_N .¹⁹ Similar behavior is exhibited by $\text{La}_{0.67}\text{Ba}_{0.33}\text{MnO}_3$. This system undergoes a $Imma \rightarrow R\bar{3}c$ first order structural phase transition, between 150 and 200 K.²² Also in this case the unit cell volume varies smoothly across the phase transition temperature.²²

The dependence of the ^{139}La signal frequency on Mn-O-Mn bonding might explain the temperature dependence of the ^{139}La NMR line shapes of $\text{La}_{0.5}\text{Ca}_{0.5}\text{MnO}_3$ in Ref. 6. In that work, the ^{139}La NMR signal at $T \approx 100$ K is shown to consist of two strongly overlapping components, whereas by increasing temperature the high frequency component decreases rapidly. According to our present results, this may indicate the formation of JT distorted (and therefore less conductive) FM regions at elevated temperatures. This is in agreement with the observations of Louca *et al.*,¹¹ who demonstrated that the number of short (Mn-O) bonds per Mn ion decreases by increasing temperature. A further observation in Ref. 6 is that similarly to the magnetization measurements, the ^{139}La NMR signal intensity in $\text{La}_{0.5}\text{Ca}_{0.5}\text{MnO}_3$ decreases rapidly below 170 K upon cooling. In the framework of the mixed FM/AFM phase the decrease of the signal intensity is explainable as an indication of the formation of AFM regions with nonresonating La nuclei. In case of formation of a uniform canted AFM state, one should rather expect a frequency shift to lower frequencies than a signal intensity decrease.

Additional information about spin ordering in $\text{La}_{1-x}\text{Ca}_x\text{MnO}_3$ was obtained with the help of ^{55}Mn NMR line shape measurements at $T = 9$ K, as shown in Fig. 5. Similarly to previous ^{55}Mn results the spectrum for $x = 0.125$ consists of two edge peaks at $\nu_1 \approx 325$ MHz and $\nu_2 \approx 420$ MHz, which according to the literature are assigned to localized AFM Mn^{4+} and Mn^{3+} , respectively,^{23,24} and a very broad central peak corresponding to intermediate Mn valence states. For $x = 0.25$ the $\nu_{1,2}$ peaks reduce drastically (only a very tiny ν_1 signal was observed), whereas a doubly peaked line centered at $\nu \approx 390$ MHz dominates the spectrum. This line corresponds to the FM metallic phase, where fast electron transfer between Mn^{3+} and Mn^{4+} ions gives a time-averaged hyperfine field. For $x = 0.33, 0.375$, and 0.5 , only the central FM peak is observed. The observation of a double FM peak instead of a single motionally narrowed one has been recently explained to originate from hole density variations across domain walls.¹⁶ According to this model, holes are energetically favored to concentrate in FM domains (a tendency balanced by Coulomb forces), thus creating a spatial variation of $B_{\text{hf}}(\text{Mn})$ across domain walls. In

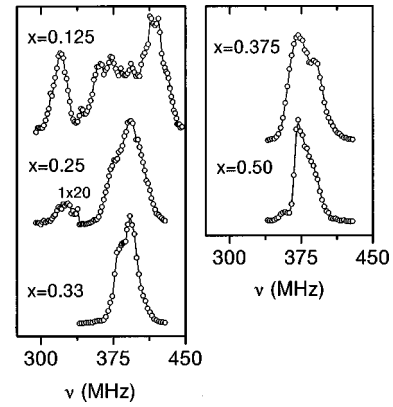


FIG. 5. Zero external magnetic field ^{55}Mn NMR spectra of $\text{La}_{1-x}\text{Ca}_x\text{MnO}_3$ for $x = 0.125, 0.25, 0.33, 0.375$, and 0.5 at $T = 9$ K. The left part of the $x = 0.25$ spectrum is magnified by a factor of 20. Spectra were obtained at very low rf level, ~ 0.1 G, which is characteristic of FM signals.

view of this fact, the low frequency FM peak is explained to originate from Mn nuclei located at the domain-domain wall interface, whereas the high frequency FM peak originates from the central region of domain walls. By increasing temperature the hole density variation is smoothed out and a single peaked FM line is observed.¹⁶ This effect might contribute to electron scattering at low temperatures.

It is noteworthy that in case of $x = 0.5$ a FM signal is observed in accordance with the ^{139}La NMR results. This supports our argument about the presence of FM islands in an AFM matrix for $x = 0.5$. Another interesting point is the complete absence of the $\nu_{1,2}$ peaks from the $x = 0.5$ system, at least for the low rf power applied. According to neutron scattering experiments in $\text{La}_{0.5}\text{Ca}_{0.5}\text{MnO}_3$ the low-temperature AFM electron spin configuration (known in the literature as CE) consists of two magnetic sublattices with independent propagation vectors, which result from charge ordering between successive Mn^{3+} and Mn^{4+} ions.⁵ Therefore, the absence of the $\nu_{1,2}$ peaks from the ^{55}Mn spectrum of the $x = 0.5$ system puts into question the generally accepted assignment of these two peaks to localized AFM $\text{Mn}^{4+,3+}$ states, similar to those observed with electron microscopy in the $x = 0.5$ system.²⁵ On the other hand, ^{55}Mn NMR measurements in other systems with Mn^{4+} at octahedral sites, such as polycrystalline Fe-Mn-Ni oxide,²⁶ exhibit a Mn^{4+} NMR frequency at ≈ 325 MHz. These findings, in conjunction with the magnetization and resistivity results shown in Fig. 1, indicate that both $\nu_{1,2}$ peaks are produced in insulating FM regions. Most probably, less mobile holes are amenable to localization effects due to impurity pinning or electron-lattice interactions, producing small FM clusters such as the $\text{Mn}^{3+}\text{-Mn}^{4+}\text{-Mn}^{3+}$ polaronic clusters proposed by Zhou *et al.*¹² In such a case the $\nu_{1,2}$ signals correspond to localized FM $\text{Mn}^{4+,3+}$ states. By increasing x conductive FM regions of undistorted Mn octahedra are created in expense of the JT distorted regions.

In summary, ^{139}La and ^{55}Mn NMR measurements in $\text{La}_{1-x}\text{Ca}_x\text{MnO}_3$ at low temperatures lead to the following conclusions. (i) At low x values polaronic lattice distortions dominate magnetotransport properties. (ii) By increasing x

FM undistorted clusters with extended hole states start to appear, and metallicity is established by a percolation transition of these undistorted clusters. (iii) For $x \approx 0.5$ it is energetically favorable for the system to break into FM and AFM regions.

Note added in proof: Recently, two very interesting works appeared [Joonghoe Dho *et al.*, Phys. Rev. B **59**, 492 (1999); K. Kumagxi *et al.*, Phys. Rev. B **59**, 97 (1999)], concerning ^{139}La NMR in $\text{La}_{1-x}\text{Ca}_x\text{MnO}_3$, which are in good agreement with the results presented in this work.

-
- ¹C. Zener, Phys. Rev. **82**, 403 (1951).
- ²P. Schiffer, A. Ramirez, W. Bao, and S.-W. Cheong, Phys. Rev. Lett. **75**, 3336 (1995).
- ³P. G. Radaelli, G. Iannone, M. Marezio, H. Y. Hwang, S.-W. Cheong, J. D. Jorgensen, and D. N. Argyriou, Phys. Rev. B **56**, 8265 (1997).
- ⁴A. Urushibara, Y. Moritomo, T. Arima, A. Asamitsu, G. Kido, and Y. Tokura, Phys. Rev. B **51**, 14 103 (1995).
- ⁵E. O. Wollan and W. C. Koehler, Phys. Rev. **100**, 545 (1955).
- ⁶G. Papavassiliou, M. Fardis, F. Milia, A. Simopoulos, G. Kallias, M. Pissas, D. Niarchos, N. Ioannidis, C. Dimitropoulos, and J. Dolinsek, Phys. Rev. B **55**, 15 000 (1997).
- ⁷G. Allodi, R. De Renzi, G. Guidi, F. Licci, and M. W. Pieper, Phys. Rev. B **56**, 6036 (1997).
- ⁸P.-G. de Gennes, Phys. Rev. **118**, 141 (1960).
- ⁹E. L. Nagaev, Usp. Fiz. Nauk **166**, 833 (1996); S. Yunoki, J. Hu, A. Malvezzi, A. Moreo, N. Furukawa, and E. Dagotto, Phys. Rev. Lett. **80**, 845 (1998).
- ¹⁰E. L. Nagaev, Phys. Lett. A **218**, 367 (1996).
- ¹¹D. Louca, T. Egami, E. L. Brosha, H. Roeder, and A. R. Bishop, Phys. Rev. B **56**, 8475 (1997).
- ¹²J.-S. Zhou, J. B. Goodenough, A. Asamitsu, and Y. Tokura, Phys. Rev. Lett. **79**, 3234 (1997).
- ¹³M. Roy, J. F. Mitchell, A. P. Ramirez, and P. Schiffer, Phys. Rev. B **58**, 5185 (1998); C. Zener, Phys. Rev. **82**, 403 (1951).
- ¹⁴G. Xiao, G. Q. Gong, C. L. Canedy, E. J. McNiff, Jr., and A. Gupta, J. Appl. Phys. **81**, 5324 (1997).
- ¹⁵I. D. Weisman, L. J. Swartzendruber, and L. H. Bennet, in *Techniques of Metal Research*, edited by E. Passaglia (Wiley, New York, 1973), Vol. VI, and references therein.
- ¹⁶G. Papavassiliou, M. Fardis, F. Milia, M. Pissas, G. Kallias, D. Niarchos, C. Dimitropoulos, and P. Scherrer, Phys. Rev. B **58**, 12237 (1998).
- ¹⁷In the case that the transferred hyperfine interaction was depending on the population of the e_g electron states, the average $\langle S \rangle$ probed by the La nuclei, and therefore the signal frequency, should decrease with x .
- ¹⁸J. Blasco, J. Garcia, J. M. de Teresa, M. R. Ibarra, J. Perez, P. A. Algarabel, C. Marquina, and C. Ritter, Phys. Rev. B **55**, 8905 (1997).
- ¹⁹P. G. Radaelli, D. E. Cox, M. Marezio, S.-W. Cheong, P. E. Schiffer, and A. P. Ramirez, Phys. Rev. Lett. **75**, 4488 (1995).
- ²⁰N. Moutis, I. Panagiotopoulos, M. Pissas, and D. Niarchos, Phys. Rev. B **59**, 1129 (1999).
- ²¹V. A. Kashin and E. L. Nagaev, Sov. Phys. JETP **39**, 1036 (1974).
- ²²P. G. Radaelli, M. Marezio, H. Y. Hwang, and S.-W. Cheong, J. Solid State Chem. **122**, 444 (1996).
- ²³G. Matsumoto, J. Phys. Soc. Jpn. **29**, 615 (1970).
- ²⁴A. Anane, C. Dupas, K. Le Dang, J. P. Renard, and P. Veillet, Appl. Phys. Lett. **69**, 1160 (1996).
- ²⁵C. H. Chen and S.-W. Cheong, Phys. Rev. Lett. **76**, 4042 (1996).
- ²⁶A. Anane, C. Dupa, K. Le Dang, J. P. Renard, P. Veillet, A. M. de Leon Guevara, F. Millot, L. Pinsard, and A. Revcolevschi, J. Phys.: Condens. Matter **7**, 7015 (1995); M. Mizoguchi and A. Tasaki, J. Phys. Soc. Jpn. **29**, 1382 (1970).